Julia Große[1]
Benjamin Dietrich[1]
Holger Martin[1]
Matthias Kind[1]
Jérôme Vicente[2]
Edme H. Hardy[3]

[1] Institut für Thermische Verfahrenstechnik, Universität Karlsruhe (TH), Germany.

[2] Ecole Polytech' Marseille, Laboratoire IUSTI – CNRS UMR 6595, Université de Provence, Marseille, France.

[3] Institut für Mechanische Verfahrenstechnik und Mechanik, Universität Karlsruhe (TH), Germany.

Research Article

Volume Image Analysis of Ceramic Sponges

The three-dimensional structure of monolithic networks such as ceramic sponges and their geometrical dimensions are part of the fundamentals necessary for investigation in most possible applications in chemical engineering. A volume imaging method must be applied to determine this structure and to measure features such as the specific surface area and the pore diameter. Magnetic Resonance Imaging was chosen for such measurements in this study. The analysis of volume images is performed with various methods based on different principles, which are compared with each other as well as with data generated by conventional techniques and from literature models.

Keywords: Cellular materials, Ceramic sponges, Magnetic Resonance Imaging (MRI), Porous media, Tomography

Received: October 26, 2007; *accepted:* December 03, 2007

DOI: 10.1002/ceat.200700403

1 Introduction

Solid sponges belong to the classification of cellular materials and are still usually referred to as "open-celled foams" in literature. The expression "foam" is typically used for cellular materials produced by the foaming of liquids, and thus, the term "sponge" seems to be more appropriate for an open-celled solid network structure. The key characteristics of solid sponges are a high and continuously accessible porosity with a low pressure drop for fluids flowing through them. In such a sponge, between 70 and 95 % of the structure consists of connected pores. The properties of cellular materials can be modified over a wide range. This flexibility of their properties led to their widespread use in different fields of application in chemical and process engineering including single- and multiphase flow. Sponges have gained further attention for thermal energy applications in recent years due to them being porous media with two continuous phases. Some examples of the applications of ceramic sponges are as solar receivers, gas burners or as alternatives for column packings. The manufacturing processes are now considered advanced enough to open a route to new industrial applications in areas ranging from lightweight construction, sound and heat insulation to energy absorption applications. Mullite, as Sheppard [1], and Schneider et al. [2] described, is a ceramic material, which is suitable for applications that require low, fixed and well-defined thermal conductivity values, e.g., as catalyst supports, hot-gas or molten-metal filters, membranes and gas burners, due to its high temperature strength, as well as its resistance to creep.

In this research project, solid ceramic sponges composed of Al_2O_3 with different pore densities and the same nominal porosity were investigated. They were produced by the Schwartzwalder process, where reticulated polymers, e.g., polyurethane foams, are coated with a ceramic suspension and sintered afterwards to remove the polymer [3, 4]. Therefore, inner cavities remain inside the struts due to the polymer precursor.

It is of high importance for the evaluation of data measured in any possible application to have reliable information about structure and size, in order to choose an appropriate characteristic length. Buciuman and Kraushaar-Czarnetzki [5] suggested some parameters for characterization of sponges by light microscopy (see Fig. 1c)). In the first instance, the diameter of the struts, t, should be measured at the finest point on the strut[1)]. Due to the high uncertainty in the determination of the pore diameters, d_p, the diameters of the faces, which connect the pores to each other, are chosen. In this study, the long and the short main axes of the ellipse, d_{f1} and d_{f2}, are measured and averaged afterwards as the arithmetic mean, d_f. Further information will be given in a forthcoming paper concerning heat transfer and characterization.

The geometrical data required for use in correlations include a value equivalent to the hydraulic diameter, which could be the diameter of the faces, a characteristic thickness of the solid, which corresponds to the diameter of the struts, or both ideally smooth and rough specific surface areas. In addition to this, several other parameters are of importance, such as the total porosity, the outer porosity, i.e., the porosity assuming the inner cavities to be solid and neglecting the matrix porosity, size of the inner cavities, orientation of the cells, tortuosity of the solid and void, as well as the distributions of the geo-

Correspondence: Dipl.-Ing. J. Große (grosse@tvt.uka.de), Institut für Thermische Verfahrenstechnik, Universität Karlsruhe (TH), D-76128 Karlsruhe, Germany.

1) List of symbols at the end of the paper.

metrical dimensions. Due to the complex structure of open-celled materials, conventional techniques are often not capable of providing all necessary information.

2 Experimental

Several samples were chosen in order to evaluate the geometrical structure of ceramic sponges. All samples were made of alumina of 99 % purity and had a nominal porosity of 80 %. Samples 1 and 2 had a nominal pore density of 20 ppi, while the sample 3 had smaller pores with a nominal pore density of 45 ppi. These differences are evident from the light microscopy images in Fig. 1.

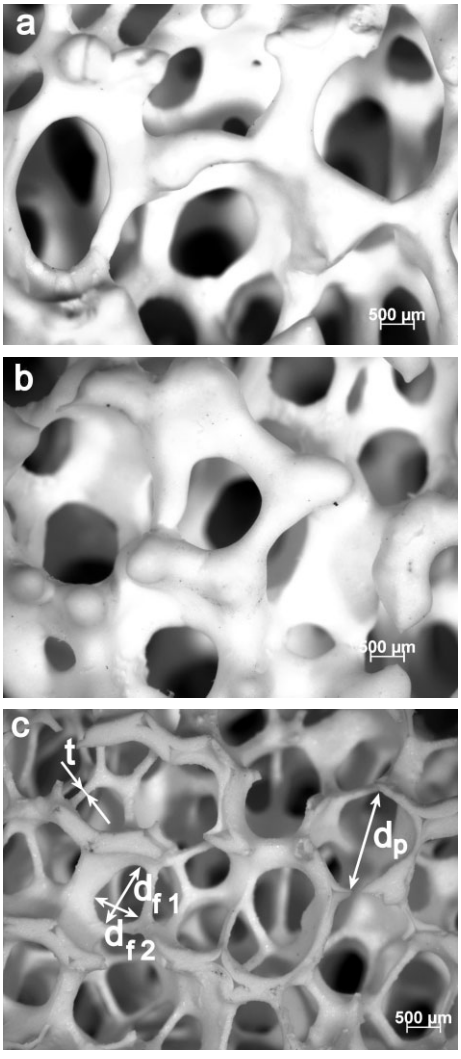

Figure 1. The chosen samples of porosity 0.8. (a) Sample 1: 20 ppi of size 14 mm × 14 mm × 50 mm; (b) Sample 2: 20 ppi of size 14 mm × 14 mm × 50 mm; (c) Sample 3: 45 ppi of size 7 mm × 7 mm × 50 mm. The characteristic lengths for the sponges are shown in part (c).

2.1 Data Acquisition

The aim of this investigation was to determine as many geometric parameters as possible for the sponges. In addition to conventional light microscopy, a volume imaging method was chosen. The combined use of both methods made a comparison and validation possible, since it is possible to detect the general structure from a three-dimensional image of the sponge. Information concerning the specific surface area of the sponge geometry can also be attained. The specific surface area cannot be determined with conventional techniques, such as measurements involving adsorption isotherms (BET), due to the high levels of roughness of the sintered ceramic material. Therefore, a volume imaging technique is required.

The technique most commonly used for three-dimensional imaging is X-ray absorption tomography, which has recently also been applied to sponges by Maire et al. [6] and Vicente et al. [7]. Another method already used in engineering is Magnetic Resonance Imaging (MRI), which has a limited resolution compared to X-ray absorption tomography but quite acceptable image quality. In addition to this, MRI facilitates the measurement of flow fields, concentration fields or even maps of anisotropic diffusion. Experiments were performed in the MRI-Laboratory, Department of Chemical and Process Engineering at the University of Karlsruhe.

Measurements for the acquisition of the three-dimensional images were performed with a Bruker Avance 200 SWB tomography (150 mm of room-temperature bore, magnetic flux density of 4.7 T, micro 2.5 gradient system generating up to 1 T/m, and birdcage resonators with diameters of 15 mm and 25 mm, respectively). A concise description of the principles and measurement methods of MRI can be found in a paper by Hardy [8]. Since the ceramic sponges produce practically no signal in standard MRI experiments, the pore space was imaged by filling it with a liquid suitable for ^{1}H-MRI measurements. For this purpose, a bubble-free filling with degassed water under vacuum was performed. Copper sulfate at a concentration of 1 g/L was added to the water allowing for faster measurements due to enhanced relaxation effects.

A fast imaging method was used to shorten acquisition time for the measurements. The so-called RARE method (rapid acquisition with relaxation enhancement, see Hardy [8]), involving a multiple spin echo, shortens the acquisition time by the so-called RARE-factor, which depends on the relaxation properties of the system. In the current case, a RARE-factor of $f_{RARE} = 16$ was used.

The resolution obtained in MRI depends on the sample size and on the number of volume elements (voxels) chosen. The sample size was adapted based on the different cell sizes with different ppi-numbers. The size of one voxel in each direction is determined by the size of the investigated field of view divided by the number of voxels. In order to achieve a reasonable acquisition time, a total data matrix size of maximum $n_x \times n_y \times n_z = 256 \times 256 \times 256$ voxels was chosen. These factors led to a resolution of 86 µm per voxel for samples 1 and 2, and of 50 µm per voxel for sample 3. Therefore, the size of the field of view was $22 \times 22 \times 22$ mm^3 for samples 1 and 2, and $12.8 \times 12.8 \times 12.8$ mm^3 for sample 3.

Good picture quality is a big challenge in volume imaging methods. The signal to noise ratio (SNR) depends on the number of averages taken for an image. At least two averages are recommended for additional compensation of experimental imperfections. In addition, a measurement with eight averages was performed on sample 2. Although there was less noise, the signal quality of the picture with two averages was already sufficient and it was no longer the limiting factor involved in the data analysis. Therefore, the faster measurement with the number of averages, $N_A = 2$, was chosen as the standard for the current measurements with a repetition time of $T_R = 1.2$ s. One measurement took approximately 2 h 45 min, as calculated by Eq. (1):

$$T = \frac{n_x \cdot n_y \cdot N_A \cdot T_R}{f_{RARE}} = \frac{256 \cdot 256 \cdot 2 \cdot 1.2\ \text{s}}{16}$$

$$= 9830.4\ \text{s} = 2\ \text{h}\ 43\ \text{min}\ 50\ \text{s} \quad (1)$$

2.2 Data Pre-Processing

Pre-processing is required prior to data analysis. Firstly, the matrix was cut to the size of the sample. Then different steps were performed in Marseille and Karlsruhe in order to investigate the influence of pre-processing on the data obtained. A summary of the different methods can be found in Tab. 1.

In Marseille, a Gaussian filter was used to eliminate most of the noise for the measurements with two averages. In addition, the Gaussian filter is helpful for pictures with a low resolution, as it smoothes the surface. Thus, an overestimation of the surface with methods working on density images due to roughness can be avoided, although the filter may slightly thicken the solid matrix. A threshold for the signal had to be chosen to distinguish regions of high signal (void filled with liquid) from regions of low signal (solid ceramic material). This was performed automatically for each slice of the matrix (see Vicente et al. [7]). The results showed no significant variation in the threshold value. Due to the application of the Gaussian filter, the ceramic structure was a little thicker compared to a direct setting of the threshold. Single spots of noise remained in the void phase, especially in cases without the Gaussian filter, and could be mistaken to be part of the solid phase. These were eliminated by identifying the groups of connected voxels, calculating their number of solid voxels and eliminating all groups with less than ten solid voxels, since they would probably be too small to be part of the solid structure. The last step of the pre-processing involved the filling of the hollow struts. This was necessary in order to determine the outer porosity of the structure. Although the measurements were performed with limited resolution, there was enough signal from the hollow struts to be visible in the volume image. The filling involved a morphological closing followed by filling all completely closed voids (see Vicente et al. [7]). The different steps of data-pre-processing are demonstrated in the upper row of Fig. 2.

Table 1. Summary of the different methods used for data pre-processing both in Marseille and in Karlsruhe.

Method Used	Marseille (M)	Karlsruhe (KA)
Filtering	Gaussian filter	None
Setting threshold	Automatically set for each slice	Minimum of histogram chosen for whole dataset
Eliminating single noise spots	Groups with less than 10 connected solid voxels	3D-cross neighborhood: noise has not more than one solid neighbor
Filling of hollow struts	Morphological closing and filling all completely closed voids	Cubic neighborhood: inner cavities have more than 14 solid neighbors

A different procedure was followed in Karlsruhe. After cutting the matrix to the size of the sample, one single threshold was chosen for all slices at the minimum between the two peaks in the histogram for the whole dataset. No filter was applied. The single spots of noise in the liquid were eliminated using an algorithm, which counted the number of solid voxels that were face-neighbors to each voxel (a three-dimensional cross with six neighbors). If a solid voxel was in contact with not more than one other solid voxel, it was determined to be

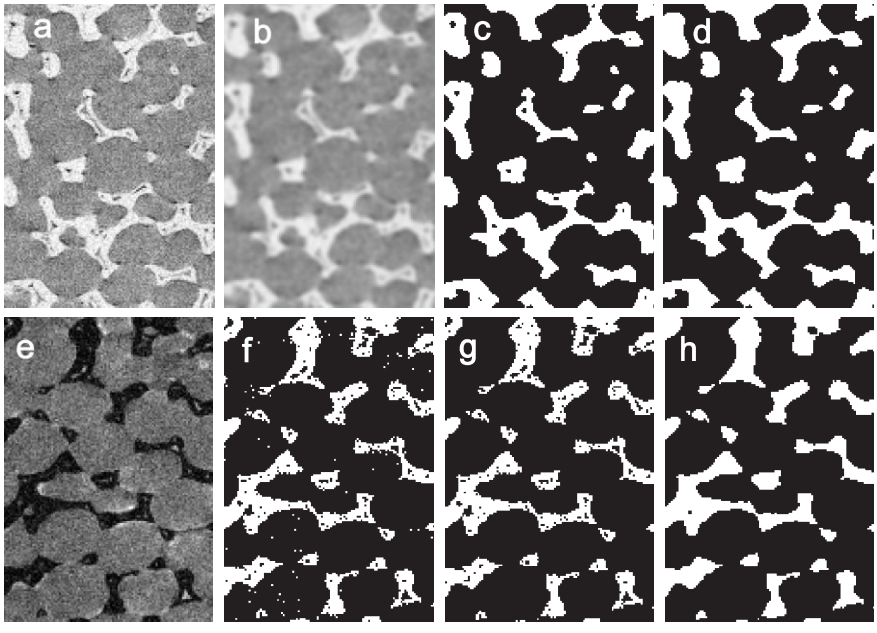

Figure 2. Data pre-processing performed on a measurement of sample 2. Method used in Marseille: (a) Cut inversed image, (b) Gaussian filtered image, (c) Setting of threshold, (d) Noise elimination + Closing morphological operation + Filling of inner void struts. Method used in Karlsruhe: (e) Cut image, (f) Setting of threshold, (g) Eliminating noise, (h) Filling inner voids in struts. All images are slices out of a 3D-matrix.

noise and eliminated. A second algorithm was developed for the filling using the fact that the voids in the struts were narrow and concave. The number of solid voxels in the cubic neighborhood (26 neighbors for each voxel) of each void-voxel was counted. If there were more than 14 solid neighbors, i.e., more than half of the surrounding voxels were solid, the voxel was identified as a void inside the struts and set to solid. This filling process was repeated three times. The complete pre-processing with the different steps as performed in Karlsruhe is visualized in the lower row of Fig. 2.

2.3 Data Analysis

The data analysis was performed on the pre-processed data using two different methods, which could be compared with each other as well as with results of light microscopy. A summary of the methods used can be found in Tab. 2. After setting the threshold and eliminating the noise, the total and the outer porosity were determined by counting the number of solid voxels both in the unfilled and filled data matrices. Following this, the specific surface area of the filled matrix was determined with two methods based on different principles, in order to validate the values found for the specific surface area.

The first method used for the purpose of validating the specific surface area was a volume segmentation combined with conventional surface rendering, as described in detail in Vicente et al. [7]. Alternatively, an elegant and efficient determination of the specific surface area using a Crofton formula was performed as a second method. Rather than reconstructing the surface, void-solid interfaces are counted and averaged along various directions. The theoretical background and the algorithms used can be found in Ohser and Mücklich [9]. Here, only the underlying Crofton formula is given, Eq. (2):

Table 2. Summary of the methods used for data analysis and conventional data.

Method Used	
Data Analysis	–
Total porosity	Counting solid voxels in unfilled data
Outer porosity	Counting solid voxels in filled data
Specific surface area 1	Volume segmentation and surface rendering
Specific surface area 2	Crofton-formula: Eq. (2)
Cell segmentation	Watershed transformation of the marker distance function
Strut thickness	Aperture diameter map for the solid
Conventional Data	
Diameters of struts and faces	Light microscopy
Density of the solid	Helium pycnometry

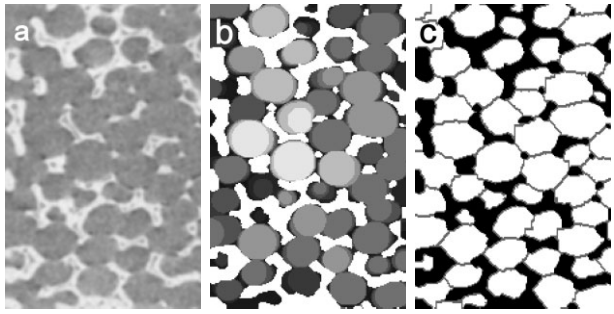

Figure 3. Example of morphological analysis performed on a measurement of sample 2. (a) Cut image, (b) Aperture diameter map image, (c) Segmented cells (cells are delimited by walls shown by the grey lines).

$$S(X) = 4 \int_{\Omega} \int \chi\left(X \cap e_{y,}\right) \, \mathrm{d}y \;\; \mu \; (\mathrm{d}\omega) \tag{2}$$

The one-dimensional Euler number, $\chi(X \cap e_{y,\omega})$ counts the number of intersections of the solid phase, X, with the line $e_{y,\omega}$ of direction ω determined by the angles α and β passing through the point y in a plane perpendicular to ω. The inner integral over all surface elements in that plane, dy, thus facilitates the calculation of the area of the "shadow" of the solid phase on that plane, taking into account the number of separated solid parts contributing locally to the shadow. The total surface, S, is obtained by averaging over the unit sphere, Ω, with $\mu(\mathrm{d}\omega) = \sin\alpha \mathrm{d}\alpha \mathrm{d}\beta/(4\pi)$. The inner integral is also denoted as the "area of the total projection" or "rose of intersections", $\wp^{\omega}$, and in this case, the Crofton formula is known as the Cauchy formula.

In addition, a segmentation of cells was performed with a watershed-transformation of the marker distance function. This made the determination of both cell shape and cell orientation possible, and gave additional information about the three-dimensional structure of the sponge, see Fig. 3. The three main axes $a > b > c$ and their orientation in terms of azimuth, φ, and elevation, θ, referring to the origin set by placing the sample in tomography were determined for each cell. From the cell volume, a diameter of a volume-equivalent sphere was calculated for each cell and averaged for the entire sample to obtain a mean pore diameter.

The thickness of the struts is a feature easily accessible in light microscopy and is useful for validation of the volume image analysis data. In order to obtain this information from volume image analysis, an aperture diameter map for the solid phase was generated as described for the void phase in Vicente et al. [7]. The density function of the distribution of the aperture diameter is bimodal, since not only the struts but also all other parts of the solid such as vertices and closed faces were taken into account. Therefore, both a Gaussian distribution for the average strut size and a Weibull distribution for the size of the vertices and other solid material were fitted to the distribution of the aperture diameter. This combination was chosen due to the fact that vertices are located at the end of struts and have a minimal size. The average size of the struts was set to the expected value from the Gaussian distribution.

2.4 Additional Data for Comparison

Microscopic measurements were performed to determine the diameter of struts and faces in order to validate the values found with volume image analysis. It was also possible to compare the values for total porosities found in MRI with values determined by measuring the size and the weight of the sample as well as the density of the solid, which was measured with helium pycnometry.

A value for the expected surface area can be calculated from the microscopy data by using the model of a dense packing of tetrakaidecahedra, as found in literature and discussed by Buciuman and Kraushaar-Czarnetzki [5], Eq. (3):

$$S_{geo} = 4.82 \frac{1}{d_f + t} \sqrt{1 - \varepsilon} \quad (3)$$

3 Results and Discussion

All measurements were analyzed as described above. The results obtained and the additional data for comparison are summarized in Tab. 3. The results for the porosity determined from MRI-data with the different pre-processing methods were consistent. The smaller values for the porosity determined with the pre-processing performed in Marseille were due to the Gaussian filter applied before the setting of the threshold. Any influence due to the setting of the threshold could be neglected, since changing the threshold by 5 % only led to a variation of 0.5 % for the outer in total as well as for the filled porosity and the specific surface area.

In general, the results from MRI were consistent with the conventional data obtained. The total porosities determined by MRI are always too low. This could be due to the insufficient resolution concerning the size of the voids inside the struts. For samples 1 and 2, the strut size corresponds to the size of four to five voxels. Inner cavities smaller than ca. 40 μm, which correspond to 10 % of the strut size, cannot be detected in these measurements. For sample 3, this effect is even more important, since the strut size corresponds to the size of three voxels. In this case, cavities smaller than ca. 25 μm cannot be measured, which corresponds to almost 20 % of the strut size. Thus, the differences between the values determined conventionally and with MRI are due to the fact that a significant portion of the inner cavities are inside the middle of the struts. With regard to the outer porosities, this effect should be of little influence, and therefore, the values found for this parameter are reasonable.

The two measurements for sample 2 show that the reproducibility of the results is very good. The differences in the porosities are due to a change in pre-processing performed in Marseille, i.e., the measurement with eight averages did not require a Gaussian filter, and therefore, only the single spots of noise were eliminated. The results for the porosity are then much closer to those determined with the pre-processing performed in Karlsruhe.

The values for the specific surface area calculated with the two different methods on data with similar pre-processing are in very good agreement. The second method using the Crofton formula leads to slightly smaller values, but the difference is smaller than 3 %. The different pre-processing leads to the same range of differences, except for the measurement with more averages, where no Gaussian filter was applied in the pre-processing. Considering these results and the results for the porosity, applying a Gaussian filter seems to thicken the structure of the sponges and perhaps leads to less reliable results.

The image analysis leads to smaller values compared with the values calculated for the geometrical surface area of the tetrakaidecahedron, although the range is similar. Nevertheless,

Table 3. Summary of the results for all samples. Sample 2 was measured with both two and eight averages. (M): values determined with the pre-processing as performed in Marseille, (KA): values determined with the pre-processing as performed in Karlsruhe.

Feature	Sample 1	Sample 2 (2 av.)	Sample 2 (8 av.)	Sample 3
Nominal Parameters				
Material	Al_2O_3	Al_2O_3	Al_2O_3	Al_2O_3
Number of pores per inch	20 ppi	20 ppi	20 ppi	45 ppi
Porosity	0.8	0.8	0.8	0.8
MRI				
Total porosity (M)	0.741	0.721	0.750	0.730
Total porosity (KA)	0.781	0.775	0.768	0.781
Outer porosity (M)	0.736	0.718	0.737	0.727
Outer porosity (KA)	0.757	0.745	0.747	0.760
Spec. surface 1 (M) (m^2/m^3)	1244	1268	1430	1982
Spec. surface 2 (M) (m^2/m^3)	1229	1247	1389	1974
Spec. surface 2 (KA) (m^2/m^3)	1187	1213	1204	1917
Mean value axis *a* (M) (μm)	2949	2924	2962	1523
Mean value axis *b* (M) (μm)	2329	2309	2321	1297
Mean value axis *c* (M) (μm)	2087	2073	2096	1159
Eq. diameter (M) (μm)	2675	2655	2679	1448
Mean strut size (M) (μm)	258	429	417	154
Conventional Data				
Mean strut size (μm)	341	358	358	127
Mean face diameter (μm)	1096	1232	1232	745
Density of the solid (g/cm^3)	3.891	3.891	3.891	3.891
Total porosity	0.814	0.800	0.800	0.856
Calc. spec. surf. (Eq. (3)) (m^2/m^3)	1458	1362	1362	2119

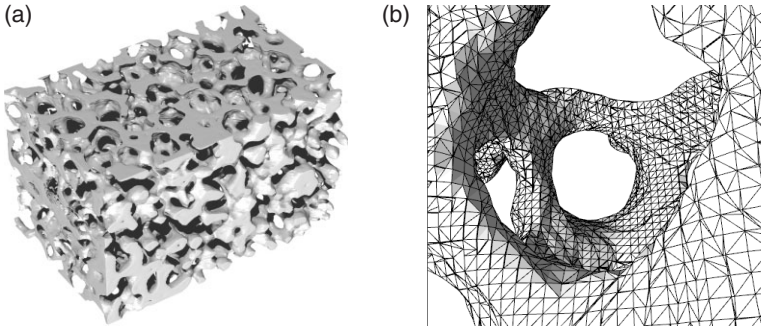

Figure 4. Geometrical surface of sample 1. (a) Reconstruction of the sample and (b) the rendered surface made of triangles.

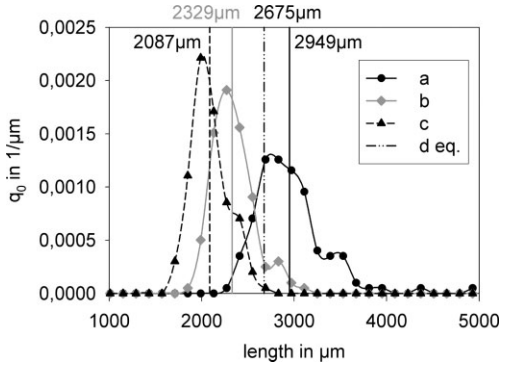

Figure 5. Density function of the distribution of twice the main axes of sample 1. The vertical lines represent the mean value of each distribution and the average diameter of the volume-equivalent sphere for all cells in the sample.

the assumption of a perfect packing of tetrakaidecahedra leads to a good agreement with the measurements and can give a first idea of the range. With further measurements, it will be possible to develop a correlation similar to Eq. (3) for the sponges.

For sample 1, a detailed analysis is now discussed as an example. The rendered surface of the sample is visualized in Fig. 4. The distributions of the lengths of the main axes of the sample generated from cell-segmentation are shown in Fig. 5. Depending on the sample analyzed, the distributions of the main axes can possess secondary peaks at smaller or bigger values. These are induced by segmentation errors or by taking incomplete cells from the border of the sample into account.

Fig. 6 shows the orientation of the cells of sample 1. The azimuth, which is the orientation in the base plane, shows clearly, that the smaller axes *b* and *c* are perpendicular to *a*. All distributions have relatively narrow peaks. The other samples lead to similar results. It is clearly visible in Fig. 5 that the cells are all elongated, since the axes *a* are nearly one and a half times longer than the axes *c*. At the same time, the axes *a* all have the same orientation within an range of 30°, which can be seen in Fig. 6. Thus, the cells of the sponge are all oriented in the same direction due to the production process, since the gravitational force causes an elongation of the bubbles during the foaming of the precursor. This direction becomes a preferential direction of the structure, such that the sponge is not really isotropic. These conclusions were confirmed by the results of all other samples and measurements.

Fig. 7 shows the distribution of the aperture diameter generated from the aperture diameter map and the fits for the struts and vertices. As the resolution of the MRI is not very fine, an average value of four voxels per strut diameter can be expected. This is normally not precise enough to make a reliable analysis. However, a qualitative analysis is possible. The regression of the fit is sufficient and the values found in MRI are close to the values found with light microscopy, so that the setting of the threshold and the elimination of noise were performed successfully.

A detailed analysis of uncertainties is out of the scope of this paper, and therefore, only a list of error sources is indicated. The uncertainties of the experimental method are due to discretization, distortions and noise. The limited sample size

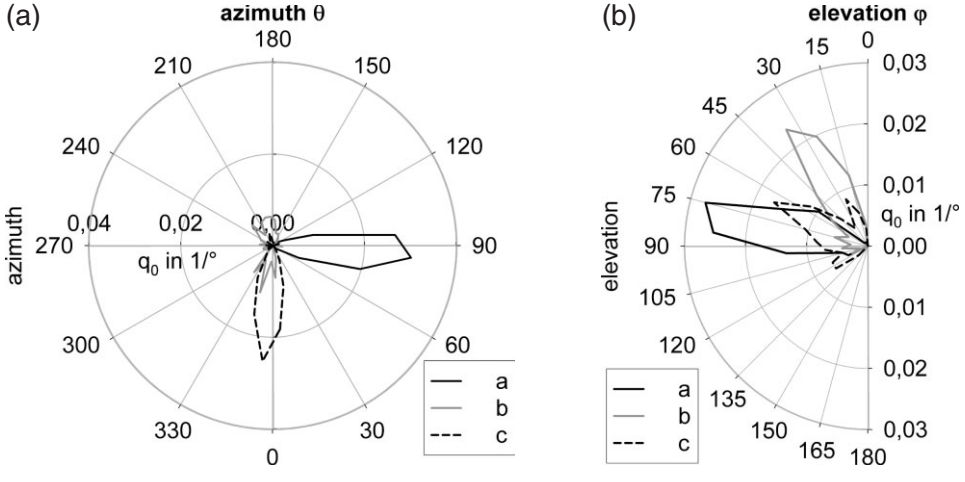

Figure 6. Orientation of the cells in sample 1 represented by the density function of the distribution of azimuth and elevation.

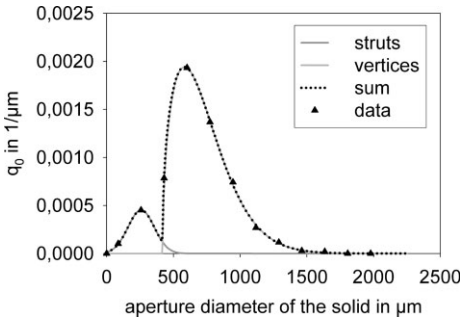

Figure 7. Distribution of the aperture diameter of the solid in sample 1 with the two fits for struts and vertices and the sum of both fitted distributions.

introduces statistical uncertainties to the calculated averaged values and distributions and leads to additional errors due to edge effects. As observed here, data pre-processing, e.g., thresholds and in particular filtering, introduce systematic errors. In addition, the techniques used here for the evaluation of the specific surface area, surface reconstruction or application of a Crofton formula, lead to slightly different results. With regard to the experimental method, distortions are not assumed to have a significant influence on the uncertainty, and measurements with different signal-to-noise ratios indicated that the noise is also not limiting the accuracy in the present study. The influences of discretization and the resolution for a given field of view might be controlled by observation of the convergence of porosity with resolution. In contrast, the specific surface area obtained depends inherently on the resolution. The influences of edge effects and limited number of geometrical objects are dealt with in the field of stochastic geometry. The effect of these methods on the relevant results can be better appreciated by applying different methods for data analysis, such as surface reconstruction and Crofton-formula based methods.

4 Conclusions

MRI was applied successfully as a volume imaging method for the characterization of ceramic sponges. It was possible to determine the geometrical specific surface area of the structure, as well as the shape and the orientation of the cells, which would otherwise be difficult to determine.

Two methods based on different principles were compared with each other and with a literature model for pre-processing as well as for determination of the specific surface areas. It was shown that the values of the specific surface area determined with the different methods were in good agreement. The influence of the pre-processing was not as significant as had been presumed. The values were all close together within less than 5 % deviation. When the values were compared with literature models it was shown that although the model of a dense packing of tetrakaidecahedra leads to bigger values than found in image analysis, they might be useful for calculating a first value when no volume imaging can be performed.

Whereas the resolution in MRI is inferior to the resolution obtainable by X-ray tomography, it was adequate to obtain the data required in the present study with sufficient accuracy. The results were in agreement with the values determined with conventional methods such as light microscopy. In addition, MRI allows the measurement of the flow field, concentrations maps or local anisotropic diffusion with the same experimental setup. The flow field results will be published in a forthcoming paper.

Acknowledgements

The authors would like to thank the German Research Foundation (Deutsche Forschungsgemeinschaft) for the financial support of Research Unit 583 "Solid Sponges – Application of Monolithic Network Structures in Process Engineering". The authors also thank Dr. Wilhelm Schabel for the initiation of this cooperation.

Symbols used

d_p	[µm]	pore diameter
d_{f1}	[µm]	long face diameter
d_{f2}	[µm]	short face diameter
d_f	[µm]	averaged face diameter
dy	[m^2]	surface element
$e_{y,\omega}$	[–]	line, direction of $\omega = (\theta, \varphi)$ passing through y
f_{RARE}	[–]	RARE-factor
n_x	[–]	size of matrix in dimension x
n_y	[–]	size of matrix in dimension y
n_z	[–]	size of matrix in dimension z
N_A	[–]	number of averages
ppi	[–]	number of pores per linear inch
$S(X)$	[m^2]	surface of solid phase X
S_{geo}	[m^2/m^3]	specific surface area
t	[µm]	strut diameter
T	[s]	measurement time
T_R	[s]	repetition time
X	[–]	solid phase
α	[°]	angle
β	[°]	angle
ε	[–]	outer porosity
θ	[°]	elevation
$\mu(d\omega)$	[–]	solid-angle element divided by 4π
φ	[°]	azimuth
$\chi(X \cap e_{y,\omega})$	[–]	one-dimensional Euler Number
Ω	[–]	unit sphere

References

[1] L. M. Sheppard, in *Ceramic Transactions: Porous Materials* (Eds: K. Ishizaki et al.), Vol. 31, American Ceramic Society, Westerville, OH **1993**.

[2] H. Schneider, K. Okada, J. Pask, *Mullite and Mullite Ceramics*, John Wiley & Sons, New York **1994**.

[3] J. Adler, G. Standke, *Keram. Z.* **2003**, *55 (6)*, 694.
[4] J. Adler, G. Standke, *Keram. Z.* **2003**, *55 (10)*, 786.
[5] F. C. Buciuman, B. Kraushaar-Czarnetzki, *Ind. Eng. Chem. Res.* **2003**, *42 (9)*, 1863.
[6] E. Maire et al., *J. Eur. Ceram. Soc.* **2007**, *27*, 1973.
[7] J. Vicente, F. Topin, J.-V. Daurelle, *Mater. Trans.* **2006**, *49 (9)*, 2195.
[8] E. H. Hardy, *Chem. Eng. Technol.* **2006**, *29 (7)*, 785. DOI: 10.1002/ceat.200600046
[9] J. Ohser, F. Mücklich, *Statistical Analysis of Microstructures in Materials Science*, John Wiley & Sons, Chichester, UK **2000**.

